Hindawi
Advances in Civil Engineering
Volume 2024, Article ID 7718335, 9 pages
https://doi.org/10.1155/2024/7718335

Research Article

Investigation of Engineering Properties and Solidification Mechanism of Loess by Sodium Silicate Alkali-Activated Coal Gangue Powder

Yang Yang,[1] **Shengsheng Yu**,[2] **Xiao Ma**,[1] **Aiping Hu**,[1] **and Ping Li**[1]

[1]*School of Civil Engineering, Longdong University, Qingyang 745000, China*
[2]*School of Civil Engineering, Lanzhou Jiaotong University, Lanzhou 730070, China*

Correspondence should be addressed to Yang Yang; yy951643570@163.com

Received 20 July 2023; Revised 29 October 2023; Accepted 29 April 2024; Published 15 May 2024

Academic Editor: Tianshou Ma

The aim of this study is to investigate the engineering properties and solidification mechanism of loess through the use of alkali-activated coal gangue powder with sodium silicate. Experimental methods and comprehensive analysis were employed to examine the effects of different proportions of alkali-activated coal gangue powder with sodium silicate on the engineering properties of loess, including mass shrinkage, compressibility, and shear strength. Additionally, scanning electron microscopy was utilized to gain in-depth insights into the interaction and solidification mechanism between loess and alkali-activated coal gangue powder. The results show that the sodium silicate alkali-activated gangue powder curing loess has significantly improved the compressive strength and shear strength of the loess. With a ratio of 7 : 2 : 1, the 28 days compressive strength of solidified loess is 1.7 MPa, and the shear strength is 67.92 kPa, which is 1.91 and 2.13 times the 28 days compressive strength and shear strength of unmixed gangue powder and sodium silicate specimens respectively. The hydration–hydrolysis reaction, ion-exchange reaction, and volcanic ash reaction of the gangue powder under an alkaline environment generated hydrides that filled the pores between soil particles, enhanced the interparticle cohesion, and made the internal structure of the specimens denser, improving the engineering performance of loess solidification. The proposed sodium silicate alkali-activated gangue powder curing loess mechanism can provide a theoretical reference for the engineering application of gangue powder and the curing modification of loess.

1. Introduction

Loess is widely distributed in Asia, Europe, America, and Africa, covering approximately 10% of the global land area [1]. However, loess possesses unique geotechnical characteristics. Macroscopically, it has developed joints, fractures, and piping channels, which contribute to significant structural behavior. Microscopically, its loose and porous structure is prone to deformation upon contact with water, exhibiting pronounced destructiveness [2]. Due to the special properties of loess, such as its susceptibility to collapse and damage under loading and wetting, the geological and ecological environment of loess plateaus is extremely fragile. It has become one of the regions with the most severe soil erosion worldwide and is also highly prone to geological hazards [3]. Since 1949, human engineering activities have intensified and resulted in various geological disasters with adverse consequences to the Loess Plateau [4, 5]. For example, secondary disasters caused by a sharp rise in the water table [6], as well as massive infrastructure damage and casualties caused by landslides [6–10]. Loess, as a typical problematic soil, has generated numerous issues in geotechnical engineering, ecological environment, and geological hazards. Therefore, employing appropriate solidification methods to enhance the physical and mechanical properties of loess and analyzing the mechanisms behind performance improvement using materials science approaches and methods have become a focal point of research in the field of loess solidification in geotechnical engineering.

Some investigations presented an early classification of loess improvement curing methods, as well as a more comprehensive discussion [11, 12]. Li et al. [13] investigated the effect of quicklime on the strength, water-stability, and

Table 1: Main chemical composition of loess (%).

SiO_2	AL_2O_3	CaO	MgO	K_2O	Fe_2O_3	Na_2O
40.31	19.03	17.36	6.73	4.5	7.52	2.05

Table 2: Main chemical composition of coal gangue powder (%).

SiO_2	AL_2O_3	CaO	MgO	K_2O	Fe_2O_3
54.21	18.03	3.37	1.46	0.98	0.59

Table 3: Main chemical composition of sodium silicate.

Na_2O (%)	SiO_2 (%)	Modulus	Stack density	Whiteness (%)	Dissolution rate S (60°C, 1%)
21.73	60.44	2.87	0.55	91.34	77

compressibility of loess. Liu et al. [14] examined the effect of NaOH and KOH on the curing of loess by sodium silicate alkali-activated fly ash-based aggregates. Li et al. [15] assessed the mechanism and strength characteristics of calcium lignosulfonate-cured collapsible loess. Xia et al. [16] investigated the compressive strength and engineering applicability of different ratios of fly ash-based materials for curing the loess soil of railway roadbeds. Some researchers studied the effect of a hydrophobic curing agent on the basic physical properties and compressive strength of solidified loess [17, 18]. Lv et al. [19] studied the microstructure and mechanism of three forms of cured saline soils, including sodium silicate, diatomaceous ash, and sodium silicate mixed with diatomaceous ash. Qian et al. [20] examined the modification of raw soil properties using a fluidized bed and calcined FGD gypsum from solid sulfur ash. Zha et al. [21] conducted a study on the engineering properties of modified expansive soils using fly ash and lime-fly ash admixtures.

It's easy to notice that most previous studies have predominantly utilized cement and lime as the binding agents for stabilizing loess. However, the conventional use of cement and lime for soil solidification carries substantial environmental consequences, which do not align with today's low-carbon development ideals. On the other hand, coal gangue, an industrial waste with limited economic value, exhibits significantly lower carbon emissions compared to traditional cement. Hence, it represents an economically viable, eco-friendly alternative for solidifying loess. In light of this, this study employs coal gangue and an alkali activator to produce a low-carbon geopolymer binding material, in lieu of cement or lime. This study investigates the impact of sodium silicate on the engineering properties of alkali-activated coal gangue powder in the solidification of loess and explores the underlying curing mechanisms. This study not only enhances coal gangue utilization and reduces cement consumption, fostering sustainable development, but also provides valuable insights into the application of geopolymer soil stabilizers in engineering. It broadens the environmental benefits and practical applications of coal gangue waste, aligning with the contemporary ethos of low-carbon development and carrying significant real-world implications.

2. Experimental Study on Solidification of Loess with Sodium Silicate Alkali-Activated Coal Gangue Powder

2.1. Materials

2.1.1. Raw Soil. The raw soil used for the test was Q3 loess from Xifeng District, Qingyang City, Gansu Province, China, with a relative density of 2.7, a plastic limit of 18%, and a liquid limit of 30.1%. The main chemical composition is shown in Table 1. The main chemical composition is shown in Table 1. The raw soil sample was passed through a 5 mm standard sieve, and the mixing water was ordinary tap water.

2.1.2. Coal Gangue Powder. The gangue powder tested in this study was provided by a building material sales department in Hebei with a density of 2.3 g/cm^3, with a specific surface area of 930 m^2/kg of ordinary coal gangue powder. The main chemical composition of ordinary gangue powder is shown in Table 2.

2.1.3. Sodium Silicate. The sodium silicate used in the test was instant powdered sodium silicate produced by a company in Qingdao. The main chemical composition is shown in Table 3.

2.2. Test Plan. The test was based on the consideration of the economical and effective range of materials when blended with different doses. Five groups of ratios were designed according to the specific conditions of the materials, as shown in Table 4.

where the water–solid ratio is the ratio of water to solid material, and the water-reducing agent is 1% of the cementitious material.

2.3. Test Methods

2.3.1. Specimen Preparation and Maintenance. The raw soil with a 5 mm sieve was dried in an oven at 110°C in accordance with the *Standard for Geotechnical Test Methods* (*GBT50123-2019*), prepared by light compaction according to the ratios shown in Table 3, and six cylindrical

Table 4: Test plan.

Sample	Raw soil (%)	Coal gangue powder (%)	Sodium silicate (%)	Water reducer (%)	Water–solid ratio (%)
JC1	100	0	0	1	22
JC2	91	5	4	1	22
JC3	84	10	6	1	22
JC4	78	15	8	1	22
JC5	70	20	10	1	22

(a) (b) (c) (d) (e)

Figure 1: 28 days apparent of each group of specimens: (a) JC1, (b) JC2, (c) JC3, (d) JC4, and (e) JC5.

compression specimens of Φ 102 mm × 116 mm were made for each group. The shear strength specimens were cut by means of a Φ 61.8 mm × 20 mm ring cutter after light compaction, and eight specimens were taken from each group. The compression and shear specimens were placed in a maintenance room for 28 days at a temperature of 20−30°C with a relative humidity of 60%–80%. A specimen from each group was selected for the compressive specimens to record the change in mass drying and shrinkage over a period of 28 days.

2.3.2. Compression Test. The specimen compression test was carried out by using a microcomputer-controlled universal testing machine to load a cylindrical compressive specimen of Φ 102 mm × 116 mm without lateral limit after 28 days of curing at a loading rate of 1 mm/min. The load and displacement of the specimen were recorded. When the load dropped to 85% of the peak load, the specimen was considered to be damaged as the end condition of the test.

2.3.3. Shear Test. The shear strength of the specimens was tested using a ZJ strain-controlled straight shear apparatus in a fast shear mode after 28 days of curing, with a shear speed of 0.8 mm/min and vertical pressures of 100, 200, 300, and 400 kPa. The cohesion and angle of internal friction of each group of specimens were calculated.

3. Evaluation of the Mechanical Performance of Solidification Loess

3.1. Specimen Apparent and Mass Dry Down Results. The specimens were kept at a temperature of 20−30°C. Figure 1 shows the appearance of the specimens at 28 days. During the maintenance period, the mass drying shrinkage of each group of specimens was recorded. The change in mass drying shrinkage of the specimens during the maintenance period was plotted, as shown in Figure 2.

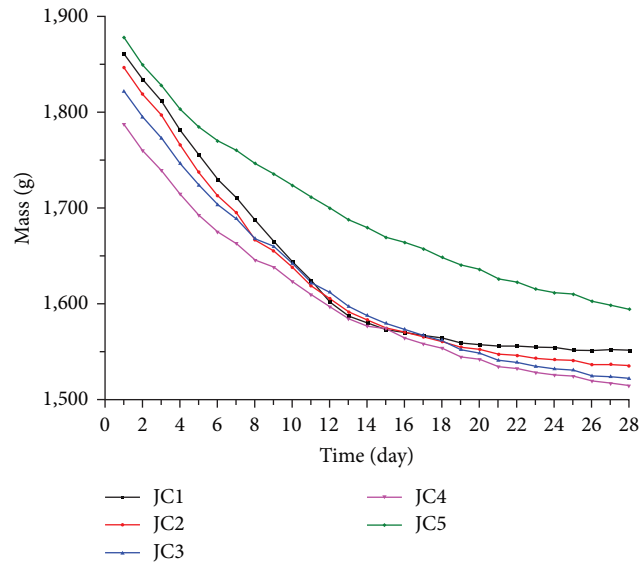

Figure 2: Changes in mass drying shrinkage during the 28-day curing period for different specimens.

Figure 1 shows that within 28 days of specimen maintenance, due to the evaporation of curing water and mineral hydration reactions, the salt accumulated on the outer surface. The outer crust thickness of specimen JC2 is only about 2 mm, and the sealing effect is not satisfactory. There is salt crystal precipitation on the outer surface, forming salt frost in the surface layer, which is most obvious around the top, as

(a) (b) (c) (d) (e)

Figure 3: Typical damage patterns for each group of specimens: (a) JC1, (b) JC2, (c) JC3, (d) JC4, and (e) JC5.

shown in Figure 1(b). The outer crust of JC5 is approximately 15 mm thick.

Figure 2 shows the mass of each group of specimens decreased as the curing time increased. The mass of JC1, JC2, JC3, JC4, and JC5 specimens decreased by 309.5, 311.3, 299.5, 273.2, and JC5283.6 g, respectively, at 28 days. There was little or no change in the height or diameter of the specimens.

3.2. Compression Test Analysis

3.2.1. Damage Characteristics of Compression Test. Using a microcomputer-controlled universal testing machine with a 1 mm/min loading rate, each group of specimens with typical damage forms is shown in Figure 3(a) load–displacement curve is shown in Figure 4. According to Figures 3 and 4, the damage pattern and damage process of each group of specimens are essentially similar. When the test machine first started to load, there was no obvious change on the surface of the specimen. As the load is gradually increased, fine cracks appear on the upper surface of the specimen mostly in an up-and-down direction. As the load continues to increase, the fine cracks gradually extend downwards and become multiple longitudinal cracks, which slowly widen in width as they extend. When the specimen is loaded to the peak load, the crack extends to the lower surface of the specimen, forming a longitudinal penetration crack on the surface. The crack width then spreads further under load, and part of the soil falls off the surface of the specimen and the specimen is damaged.

3.2.2. Compression Test Results. Specimen compression test results for Table 5 can be seen as follows: specimens mixed with coal gangue powder and sodium silicate curing loess have improved compressive strength, while specimens not mixed with coal gangue powder and sodium silicate curing loess exhibit compression strengths of 1.13, 1.07, 1.64, and 1.91 times, respectively. The compressive strength of the modified raw soil specimens in combination with 20% coal gangue powder and 10% sodium silicate (JC5 group) was the highest, reaching 1.7 MPa. The results show that the compressive strength of the solidified loess specimens can be improved by sodium silicate alkali-activated coal gangue powder under the condition of reasonable dosing. The ductility ratio of each group of specimens (JC2–JC5) mixed with coal gangue powder and sodium silicate curing loess is reduced compared with the ductility ratio of JC1 group specimens not mixed with coal gangue powder and sodium silicate curing loess, which are 87%, 89%, 96%, and 86% of JC1 group specimens. In comparison to the ductility ratio of JC1 group specimens, the ductility ratios of each group of specimens (JC2-JC5) mixed with gangue powder and sodium silicate solidified loess were 87%, 89%, 96%, and 86%, respectively, for the JC1 group specimens. Mixing coal gangue powder with sodium silicate curing loess will reduce the ductility ratio, but the reduction is not large, just 15%.

3.3. Shear Test Analysis. Figures 5 and 6 show the shear test specimens and post-shear test specimens for each group, and the shear strength versus vertical pressure curves for each group of specimens are shown in Figure 7. The linear fitting analysis of the curve in Figure 7 suggests that the cohesive forces of the specimens in the JC1 to JC5 groups are 31.87, 34.15, 40.61, 59.76 and 67.92 kPa respectively; the internal friction angles are 11.34°, 10.05°, 12.83°, 10.23°, 10.23°, and 15.59°, respectively. A close angle of internal friction exists between each group of specimens, with the smallest cohesive force of the JC1 group specimens, the largest cohesive force of the JC5 group specimens, which is 2.13 times greater than the cohesive force of the JC1 group specimens, and an enhanced cohesive force is observed for sodium silicate alkali-activated gangue powder curing loess.

4. Solidification Mechanism of Loess by Sodium Silicate Alkali-Activated Coal Gangue Powder

To further investigate the solidification mechanism of sodium silicate alkali-activated coal gangue powder solidified loess, specimens were taken from the core and shell parts of each group of specimens after the destruction of the compressive performance test, placed in anhydrous ethanol to terminate hydration, vacuum-dried and the block samples were gold sprayed and tested using a Gemini 300 (ZEISS, Germany) scanning electron microscope to analyze their microscopic morphology.

Figures 8 and 9 show the core and shell parts of the specimens in the JC1 to JC5 groups at 2,000x typical microscopic scanning electron microscopy (SEM) photographs,

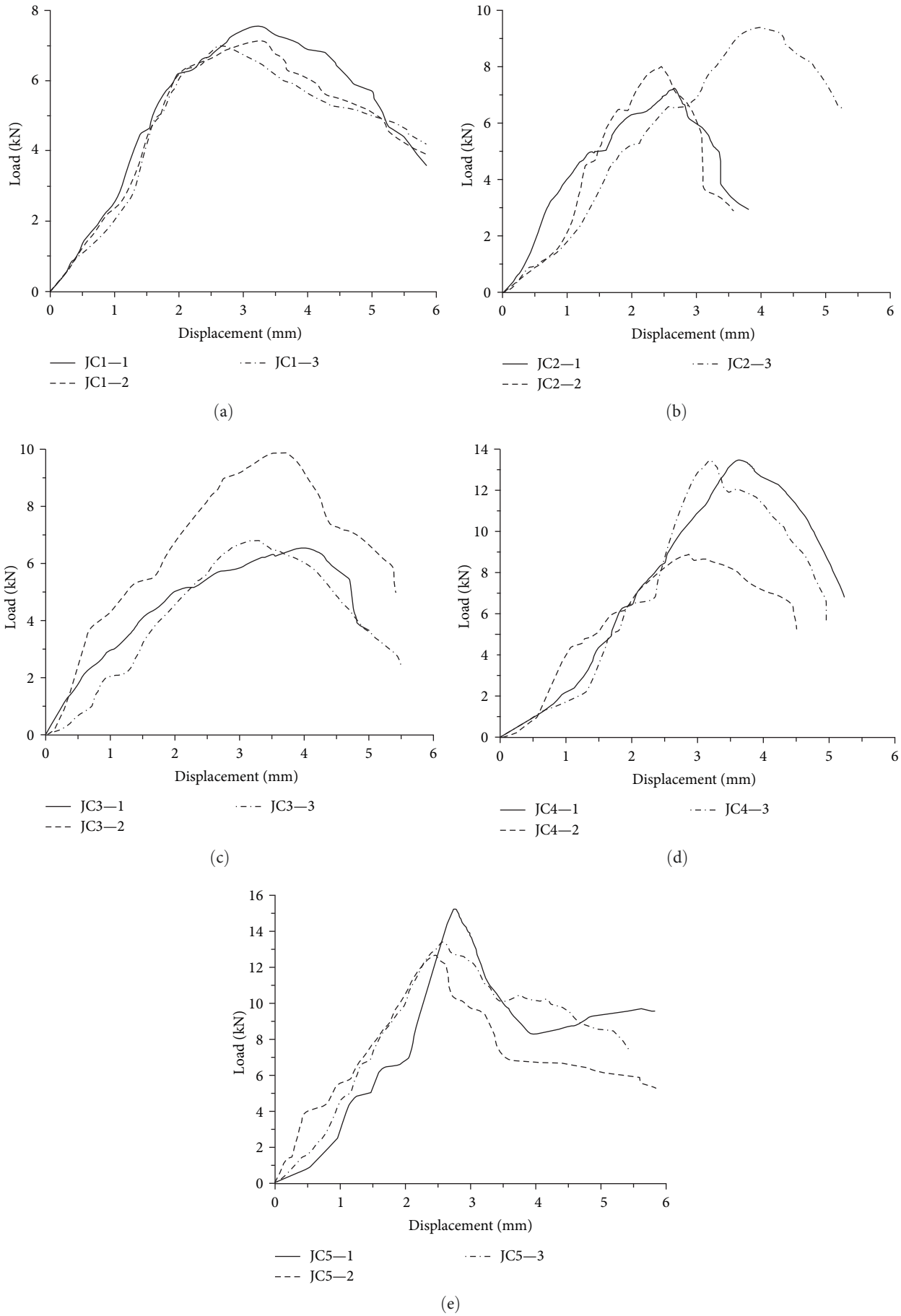

Figure 4: Load-displacement curves for each group of specimens: (a) JC1, (b) JC2, (c) JC3, (d) JC4, and (e) JC5.

Table 5: Compression test results for specimens.

Sample	Mean peak load (kN)	Mean peak displacement (mm)	Mean limit displacement (mm)	Compressive strength			Ductility ratio
				Mean (MPa)	Standard deviations	Coefficient of variation	
JC1	7.23	3.061	4.062	0.89	0.035	0.039	1.33
JC2	8.22	3.025	3.506	1.01	0.134	0.133	1.16
JC3	7.77	3.609	4.299	0.95	0.227	0.239	1.19
JC4	11.97	3.231	4.177	1.46	0.325	0.222	1.29
JC5	13.86	2.587	2.981	1.70	0.164	0.097	1.15

Figure 5: Shear test specimens.

Figure 6: Specimen form after shear test.

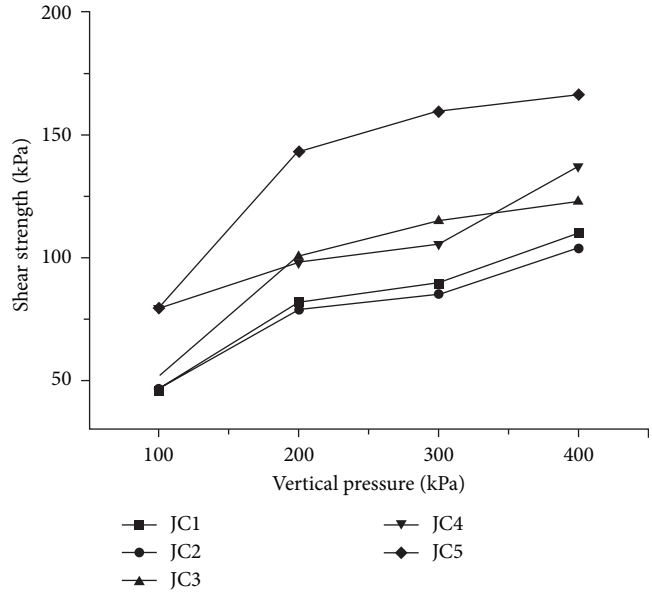

Figure 7: Shear strength versus vertical pressure curve for each group of specimens.

respectively. According to the figures, JC1 group specimens are not mixed with curing materials, the soil structure is loose, particles are arranged in a disorderly manner, and there are more voids in the soil. As sodium silicate and coal gangue powder are added to the JC2 to JC5 group specimens and mixing is increased, coal gangue powder not only performs a microaggregate filling and physical filling role but also in an alkaline environment, AL—O and Si—O bonds in coal gangue powder will be dissolved, and silicon and aluminum ion monomer will be continuously dissolved. Dissolved ions such as $(SiO_4)^{4-}$ and $(AlO_4)^{5-}$ combine with cations Ca^{2+} to undergo a volcanic ash reaction, forming a cementitious material mainly composed of silicon and aluminum-hydrated calcium silicate ($Ca{\cdot}nSiO_2{\cdot}mH_2O$) and hydrated calcium aluminate ($Ca{\cdot}nAl_2O_3{\cdot}mH_2O$), further filling of soil pores within the raw soil forms strong binding and bonding forces, thus increasing the strength of cured soil. As well, under alkaline conditions, with appropriate levels of SO_4^{2-} and Ga^{2+}, calcium aluminates ($3CaO{\cdot}Al_2O_3{\cdot}3CaSO_4{\cdot}mH_2O$) may be produced with the active silica-aluminous material. The needle-like rods seen in Figures 8(d), 8(e), 9(d), and 9(e) may be hydration products such as calcium alumina ($3CaO{\cdot}Al_2O_3{\cdot}3CaSO_4{\cdot}mH_2O$), which cross and embed into each other as the specimen ages, causing the material voids to be filled and improving the internal compactness of the cured soil sample. The addition of water-reducing agents in the cured soil sample system will

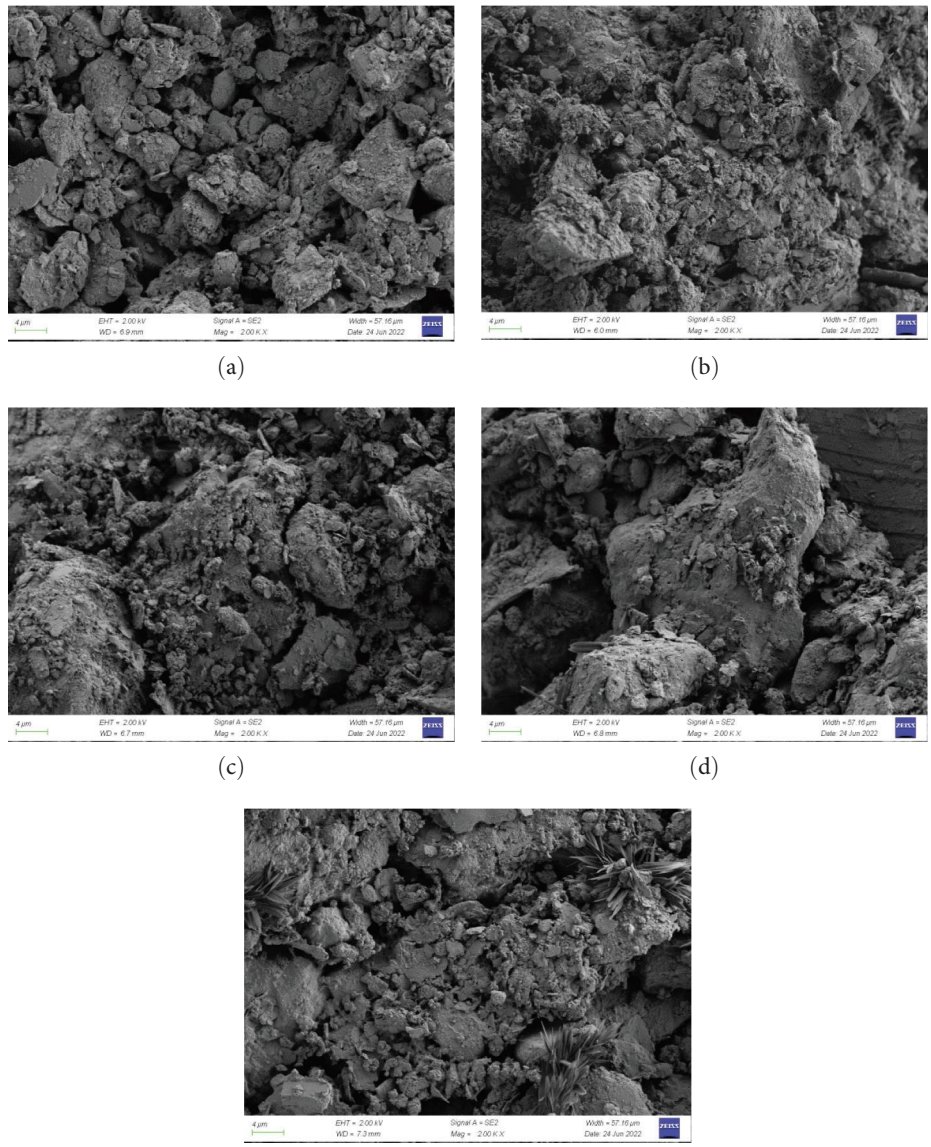

(a) (b) (c) (d) (e)

Figure 8: SEM images of the core of each group of specimens at 28 days: (a) JC1, (b) JC2, (c) JC3, (d) JC4, and (e) JC5.

further exert a dispersing and lubricating effect on the gangue powder and soil in an alkaline environment, reducing the amount of water used in curing and the porosity after curing, thus enhancing the engineering performance of the sodium silicate alkali-activated gangue powder solidified loess.

5. Conclusions

The compression and shear strength development of loess using sodium silicate alkali-activated gangue powder as curing material was studied, and its microstructure was tested. The following conclusions are drawn:

(1) The compression strength of the loess was greatly improved by using sodium silicate alkali-activated gangue powder. With the increase of sodium silicate and gangue powder, the overall compression strength of loess tends to increase; in the ratio of loess, gangue powder, and sodium silicate is 7 : 2 : 1 (JC5 group specimens), the average compression strength of loess specimens is the highest, reaching 1.7 MPa, which is 1.91 times the compressive strength of JC1 group specimens.

(2) The sodium silicate alkali-activated gangue powder curing loess has a great improvement on the shear strength of loess. In the ratio of loess, gangue powder, and sodium silicate was 7 : 2 : 1 (JC5 group specimens), the cohesive force of solidified loess specimens was the highest, and the angle of internal friction was also the largest, reaching 67.92 kPa, which was 2.13 times as much as in JC1 group specimens.

(3) Sodium silicate alkali-activated gangue powder curing loess mechanism is due to the alkaline conditions; gangue powder occurs in the hydration hydrolysis

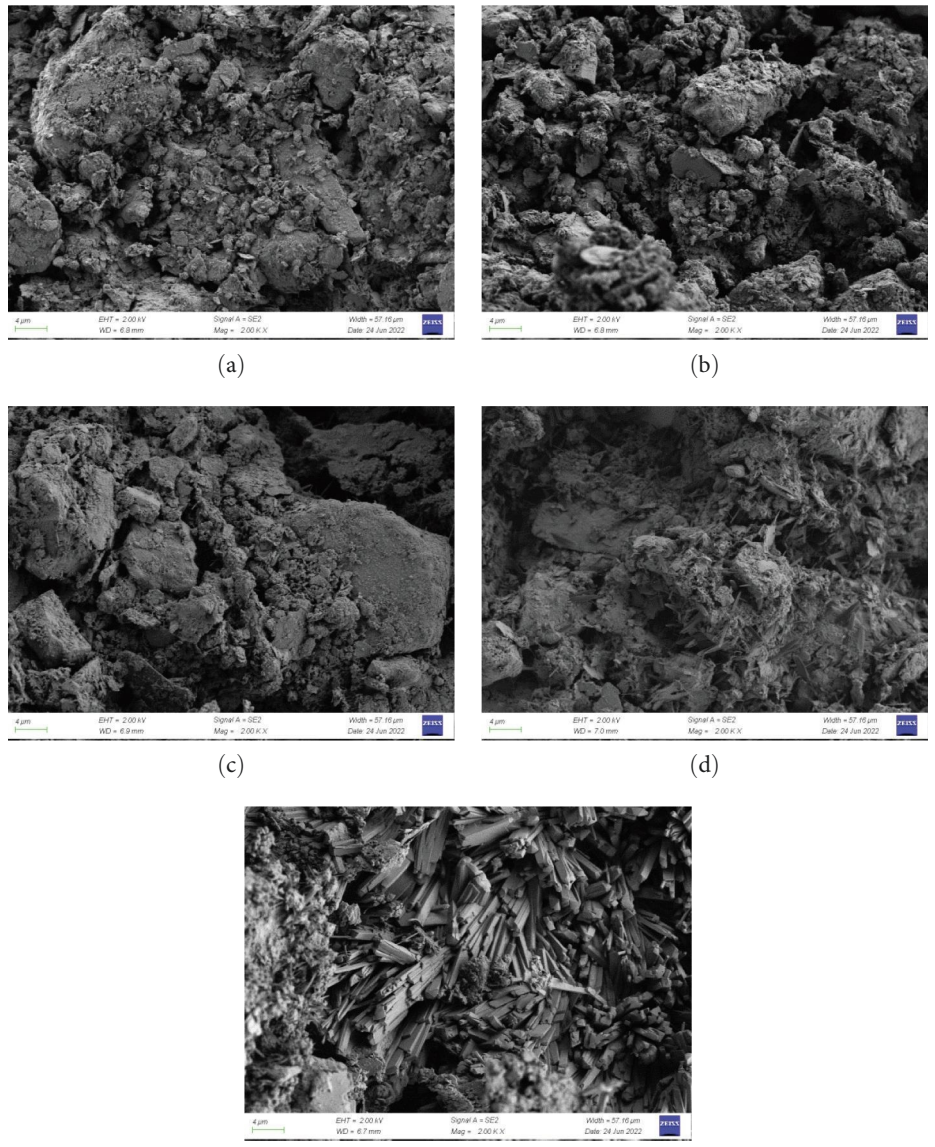

(a) (b) (c) (d) (e)

Figure 9: SEM images of the shell of each group of specimens at 28 days: (a) JC1, (b) JC2, (c) JC3, (d) JC4, and (e) JC5.

reaction, ion exchange effect, and volcanic ash reaction generated hydrides fill the pores between the soil particles. This enhances the cohesion between the particles, so that the internal structure of the specimen is more dense, so that the engineering properties of solidified loess are enhanced.

Data Availability

The data used to support the findings of this study are available from the corresponding author upon request.

Conflicts of Interest

The authors declare that they have no conflicts of interest regarding the publication of this paper.

Acknowledgments

This study received financial support from the Science Foundation for Youths of Gansu Province, China (22JR5RM212), the Natural Science Foundation of Gansu Province, China (21JR11RM052), the Innovation Foundation of Department of Education of Gansu Province, China (2022A-136), the Natural Science Foundation of Qingyang City, China (QY2021A-F023), and the Construction Technology Project of Gansu Province, China (JK2021-56).

References

[1] Y. Li, W. Shi, A. Aydin, M. A. Beroya-Eitner, and G. Gao, "Loess genesis and worldwide distribution," *Earth-Science Reviews*, vol. 201, Article ID 102947, 2020.

[2] J. Peng, X. Tong, S. Wang, and P. Ma, "Three-dimensional geological structures and sliding factors and modes of loess

landslides," *Environmental Earth Sciences*, vol. 77, no. 19, Article ID 675, 2018.

[3] E. Derbyshire, "Geological hazards in loess terrain, with particular reference to the loess regions of China," *Earth-Science Reviews*, vol. 54, no. 1–3, pp. 231–260, 2001.

[4] J. Peng, S. Wang, Q. Wang et al., "Distribution and genetic types of loess landslides in China," *Journal of Asian Earth Sciences*, vol. 170, pp. 329–350, 2019.

[5] C. H. Juang, T. Dijkstrab, J. Wasowskic, and X. M. Meng, "Loess geohazards research in China: advances and challenges for mega engineering projects," *Engineering Geology*, vol. 251, pp. 1–10, 2019.

[6] J. M. Wang, *The Theory and Application of Structural Joints in Loess*, China Water and Power Press, Beijing, 1996.

[7] C. Kang, F. Y. Zhang, F. Z. Pan, J. B. Peng, and W. J. Wu, "Characteristics and dynamic runout analyses of 1983 Saleshan landslide," *Engineering Geology*, vol. 243, pp. 181–195, 2018.

[8] J. Q. Zhuang and J. B. Peng, "A coupled slope cutting—a prolonged rainfall-induced loess landslide: a 17 October 2011 case study," *Bulletin of Engineering Geology and The Environment*, vol. 73, no. 4, pp. 997–1011, 2014.

[9] Z. Duan, W. C. Cheng, J. B. Peng, Q. Y. Wang, and W. Chen, "Investigation into the triggering mechanism of loess landslides in the south Jingyang platform, Shaanxi province," *Bulletin of Engineering Geology and The Environment*, pp. 1–12, 2018.

[10] X. Yang, J. M. Na, G. A. Tang, T. T. Wang, and A. X. Zhu, "Bank gully extraction from DEMs utilizing the geomorphologic features of a loess hilly area in China," *Thrust Belts and Foreland Basins: From Fold Kinematics to Hydrocarbon Systems*, vol. 13, no. 1, pp. 151–168, 2019.

[11] D. Evstatiev, "Loess improvement methods," *Engineering Geology*, vol. 25, no. 2–4, pp. 341–366, 1988.

[12] Y. Zhang, Y. Yao, W. Du, and H. Zhou, "Experimental study on improvement design of loess curing in engineering environment," *Bulletin of Engineering Geology and the Environment*, vol. 80, no. 4, pp. 3151–3162, 2021.

[13] P. Li, H. S. Li, H. Q. Liu, and X. L. Wang, "Application for quick lime improving strength of loess subgrade," *Advanced Materials Research*, vol. 168–170, pp. 2678–2682, 2010.

[14] H. M. Liu, L. M. Wang, and P. Gao, "The mechanical properties of cement reinforced loess and pore microstructure characteristics," *Applied Mechanics and Materials*, vol. 527, pp. 25–30, 2014.

[15] G. Li, X. Hou, W. Ma, and F. Wang, "Mechanical properties of loess treated by calcium lignosulfonate," in *Recent Advances in Geo-Environmental Engineering, Geomechanics and Geotechnics, and Geohazards, Advances in Science, Technology & Innovation*, pp. 287–289, Springer International Publishing, Cham, 2019.

[16] Q. Xia, Y. H. Yang, and X. Geng, "Experimental study on flyash-lime or flyash-cement loess filling," *Journal of Lanzhou Jiaotong University*, vol. 3, pp. 40–43 47, 2008.

[17] H. Y. Zhang, C. B. Lin, and Y. M. Sheng, "Experimental study of engineering properties of loess reinforced by consolid system," *Chinese Journal of Rock Mechanics and Engineering*, vol. 34, pp. 3574–3580, 2015.

[18] H. Y. Zhang, Y. Peng, X. W. Wang, and C. B. Lin, "Water entrance-and-release ability of loess soil modified by consolid system," *Rock and Soil Mechanics*, vol. 37, pp. 19–26, 2016.

[19] Q. F. Lv, Z. S. Wang, J. F. He, S. X. Wang, and G. Zhou, "Microstructure of saline soil solidified with alkali-activated geopolymer," *Journal of Yangtze River Scientific Research Institute*, vol. 37, no. 1, pp. 79–83, 2020.

[20] J. S. Qian, Q. Wang, X. W. Jia, and A. T. Bie, "Research on preparation of adobe materials with desulfurized wastes from coal-fired power plant," *New Building Materials*, vol. 36, no. 2, pp. 28–31.

[21] F. S. Zha, S. Y. Liu, and Y. J. Du, "Experiment on improvement of expansive clays with lime-fly ash," *Journal of Southeast University*, vol. 2, pp. 339–344, 2007.